Composition-dependent spin-phonon coupling in mixed crystals of the multiferroic manganite $Eu_{1-x}Y_xMnO_3$ ($0 \leq x \leq 0.5$) studied by Raman spectroscopy

S. Issing,[1,*] A. Pimenov,[2] V. Yu. Ivanov,[3] A. A. Mukhin,[3] and J. Geurts[1]
[1]*Physikalisches Institut (EP3), Universität Würzburg, 97074 Würzburg, Germany*
[2]*Physikalisches Institut (EP4), Universität Würzburg, 97074 Würzburg, Germany*
[3]*General Physics Institute, Russian Academy of Sciences, 119991 Moscow, Russia*
(Received 4 August 2009; revised manuscript received 12 November 2009; published 27 January 2010)

Yttrium substitution in $Eu_{1-x}Y_xMnO_3$ allows a quasicontinuous tuning of the lattice and magnetic properties of this multiferroic manganite without magnetic interference of rare-earth ions. In order to investigate the composition dependence of the spin-phonon coupling we employ polarized Raman scattering of orthorhombic mixed crystals of $Eu_{1-x}Y_xMnO_3$ ($0 \leq x \leq 0.5$) in the 10–300 K temperature range. Phonon frequency shifts and mode-mixing effects occur, depending on the average rare-earth ion radius determined by the concentration of Eu^{3+} and Y^{3+}. Moreover, we observe a strong spin-phonon coupling with systematic composition dependence. It manifests itself as a mode-specific softening of the phonon modes in the temperature range of the magnetic ordered phases. The spin-phonon coupling is weakened for increasing Y contents but remains nonzero also in the incommensurate spiral magnetic phase, which occurs for $0.3 \leq x \leq 0.5$. Thus for this class of manganites we report the observation of spin-phonon coupling in an ordered magnetic phase without ferromagnetic ordering within the MnO_2 plane. Additionally for known sublattice magnetization quantitative values of the spin-phonon coupling constant are derived. Our results prove the suitability of phonons as a sensitive probe for the spin-spin correlation.

DOI: 10.1103/PhysRevB.81.024304 PACS number(s): 75.47.Lx, 75.50.Ee, 78.30.−j, 63.20.−e

I. INTRODUCTION

Multiferroic materials have received quite a lot of attention in the recent years.[1,2] Among these materials the class of orthorhombic perovskites $RMnO_3$ (e.g., R=Gd, Tb, Dy, or Eu:Y) represents a model system which allows the study of the impact of an increasing crystalline distortion which leads to magnetic frustration and to the appearance of a long-range ferroelectric order.[3,4]

The origin of this crystalline distortion can be traced back to the ionic radii of the rare-earth ions. Their relatively small radius causes a deviation from the ideal cubic perovskite structure (space group $Pm\bar{3}m$) and therefore a lowered crystal symmetry is obtained (orthorhombically distorted structure: space group $Pnma$). This leads to a unit cell with 20 atoms and the occurrence of 24 Raman active phonon modes.[5] Thus Raman activity is in a way a measure of the orthorhombic distortion from the ideal cubic structure in perovskites. The distortion can be increased in two ways: (i) stepwise by successively using rare-earth elements with smaller ionic radius (from La^{3+} to $Pr^{3+}, \ldots, Eu^{3+}$, $Gd^{3+}, Tb^{3+}, Ho^{3+}$) (Ref. 6) or (ii) quasicontinuously by the tuning of the average rare-earth ionic radius using partial substitution of the R^{3+} ion by increasing fractions of an isoelectric ion with a smaller ionic radius. Beside randomly distributed local distortions, this results in an effective decrease in the rare-earth ion radius. For example by the partial substitution of Eu^{3+} by Y^{3+} in $Eu_{1-x}Y_xMnO_3$ the average R^{3+} ion radius can be tuned in the range from Eu^{3+} via Gd^{3+} to Tb^{3+} for Y concentrations of $0 \leq x \leq 0.5$.[7,8]

Along with the crystalline orthorhombic distortion goes an increasing magnetic frustration which leads to a suppression of the A-type antiferromagnetic (AFM) order. It is replaced by an incommensurate phase which can lead to multiferroicity due to a breaking of inversion symmetry by the spin system and therefore to the appearance of ferroelectricity. This effect was found for both the stochiometric (e.g., $TbMnO_3$ and $DyMnO_3$) and the mixed systems ($Eu_{1-x}Y_xMnO_3$ with $x \geq 0.2$).[8,9] The intimate coupling of magnetic and dielectric order was shown by Pimenov *et al.*[10] who proved the existence of a magnetoelectrically coupled elementary excitation in $GdMnO_3$ and $TbMnO_3$—the electromagnon. It was also shown that a transfer of spectral weight between electromagnon and phonon can be induced by applying a magnetic field.[11] $Eu_{1-x}Y_xMnO_3$ takes a special position in this class of compounds for two reasons: first its average rare-earth ionic radius and thus the orthorhombic distortion of the unit cell can be quasicontinuously tuned and second there is no magnetic contribution by Eu^{3+} and Y^{3+}.[8]

The existence of a strong spin-phonon coupling in the A-type AFM phase in orthorhombic $RMnO_3$, which leads to a significant phonon softening, was evidenced by temperature-dependent Raman spectroscopy.[12] It was further observed in RMn_2O_5 compounds with the same experimental technique.[13,14] While data on crystalline $RMnO_3$ samples are available for a variety of rare-earth elements, for $EuMnO_3$ only studies of polycrystalline and ceramic samples were reported.[12,15] As the rare-earth ion radius was decreased in these studies, the A-type AFM order as well as the phonon softening were reduced and starting from Eu^{3+} no phonon softening was found. This fact is surprising because in $EuMnO_3$ and $GdMnO_3$ there is still an A-type AFM phase below T_N=46 K and T_N=26 K, respectively,[9] and, therefore, phonon softening below T_N should be observable.

In order to systematically study the effect of rare-earth substitution in a magnetoelectric manganite and to clarify whether the absence of phonon softening in the previous studies may be due to the polycrystallinity of the samples,

we report in this study the temperature-dependent polarized Raman measurements on mixed crystals of $Eu_{1-x}Y_xMnO_3$. Our results show that phonon softening in these crystals is present, which strongly supports the assumption that phonon softening in orthorhombic manganites is most pronounced in samples with an *A*-type AFM phase. But our results also clearly show that a weakened spin-phonon coupling does exist in the incommensurate magnetic phases. We will discuss these findings as a possibility to use Raman spectroscopy as a sensitive probe for the spin-spin correlations.

II. EXPERIMENTAL DETAILS

$Eu_{1-x}Y_xMnO_3$ mixed crystals with Y content of $x=0$, 0.1, 0.2, 0.3, 0.4, and 0.5 were grown by a floating-zone method with radiation heating. Details of the growth procedure[16] as well as characterization with x-ray diffraction (XRD), magnetic, dielectric susceptibility,[8] and terahertz spectroscopy[17,18] can be found in literature. The XRD results of Ref. 8 clearly show that no secondary phases exist for the investigated Y concentrations. Additionally the results of the optical measurements concerning the investigation of the electromagnons[17,18] prove that an unambiguous uniform orientation of the crystal axes throughout the whole sample exists, ruling out a possible twinning of the investigated samples. All samples are b-cut with the exception of $x=0.1$ which is a-cut (all in *Pnma* notation). Consequences for symmetry selection rules in Raman scattering will be discussed in the next section.

The Raman spectra were measured in backscattering geometry using a Dilor XY 110 triple spectrometer (spectral resolution 1 cm^{-1}) equipped with an Olympus BHT microscope and a liquid-nitrogen cooled charge coupled device detector. Temperature dependent measurements were performed in the range from 10 to 300 K employing a CryoVac continuous flow cryostat. Laser light of a He-Ne laser (wavelength 632.8 nm) was focused on the sample through a 50 $\times$ ultralarge working distance objective keeping the irradiance power low (≈ 2 mW/μm^2) thus avoiding local heating.

III. RESULTS AND DISCUSSION

Figure 1 shows the polarized Raman spectra of all $Eu_{1-x}Y_xMnO_3$ samples obtained at $T=10$ K in $b(a,a)\bar{b}$ and $b(a,c)\bar{b}$ scattering geometry in Porto's notation,[19] giving access to the A_g and B_{2g} phonons, respectively.[5] The strongest Raman modes occur for tilting, rotation or stretching of the MnO_6 octahedra. The Raman lines are notated according to Iliev *et al.*[5] The corresponding main atomic displacement patterns of the eigenmodes are shown in Fig. 2. In agreement with the literature data the $B_{2g}(1)$ mode is assigned to a symmetric stretching of the MnO_6 octahedra, the $A_g(1)$ and $A_g(3)$ to a mixture of an antisymmetric stretching and a MnO_6 bending, $A_g(4)$ to a MnO_6 rotation, $B_{2g}(2)$ to a scissorslike stretching and $B_{2g}(3)$ to a MnO_6 bending.[6]

For b-cut samples B_{2g} phonons are allowed in $b(a,c)\bar{b}$ or $b(c,a)\bar{b}$ and A_g phonons in $b(a,a)\bar{b}$ or $b(c,c)\bar{b}$ scattering configuration, respectively.[5] The selection rules are almost

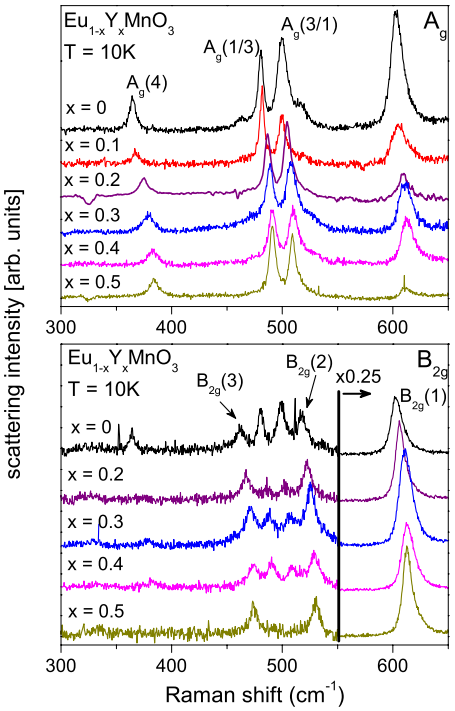

FIG. 1. (Color online) Polarized Raman spectra of $Eu_{1-x}Y_xMnO_3$ obtained at $T=10$ K in A_g (upper frame) and B_{2g} (lower frame) symmetry. The A_g scattering configuration is $b(a,a)\bar{b}$ and B_{2g} is $b(a,c)\bar{b}$. For $Eu_{0.9}Y_{0.1}MnO_3$ the scattering configurations are $a(c,c)\bar{a}$ (A_g) and $a(b,c)\bar{a}$ (B_{1g} not shown here).

ideally fulfilled for $Eu_{0.8}Y_{0.2}MnO_3$ and $Eu_{0.5}Y_{0.5}MnO_3$, which were polished up to optical degree. The occurrence of symmetry forbidden phonons in the spectra of the other samples is attributed to a nonideal polishing of the sample surface. Y doping does not seem to have a major impact on the fulfillment of the selection rules as the highest leakage of the $B_{2g}(1)$ mode occurs for the undoped $EuMnO_3$ sample which has the highest residual surface roughness of the whole sample series. Our claim of surface roughness as the reason for lifting the symmetry selection rules is substantiated in Fig. 3 by comparing polished and unpolished areas of the same sample: $Eu_{0.8}Y_{0.2}MnO_3$. In both scattering configurations $b(a,a)\bar{b}$ (A_g) and $b(a,c)\bar{b}$ (B_{2g}) the selection rules are well fulfilled for the polished area while symmetry forbidden peaks strongly occur from the rough area. The latter are marked by asterisks, the most prominent representative is the $B_{2g}(1)$ peak in A_g symmetry.

For $Eu_{0.9}Y_{0.1}MnO_3$ ($x=0.1$) the detection of B_{2g} phonons is not possible due to selection rules because this sample is a-cut. For an a-cut sample, the scattering configuration $a(b,c)\bar{a}$ and the selection rules allow only B_{1g} phonons. These could however not be detected as they have a very weak Raman activity in agreement with the phonon spectra of stoichiometric $RMnO_3$.[5] Only due to a quite rough sample surface the violation of selection rules is possible and the very strong $B_{2g}(1)$ phonon can be observed in A_g symmetry (see Fig. 1).

The different rare-earth ion radii of 1.13 Å for Eu^{3+} and 1.06 Å for Y^{3+} (Ref. 21) lead to a clear decrease in the

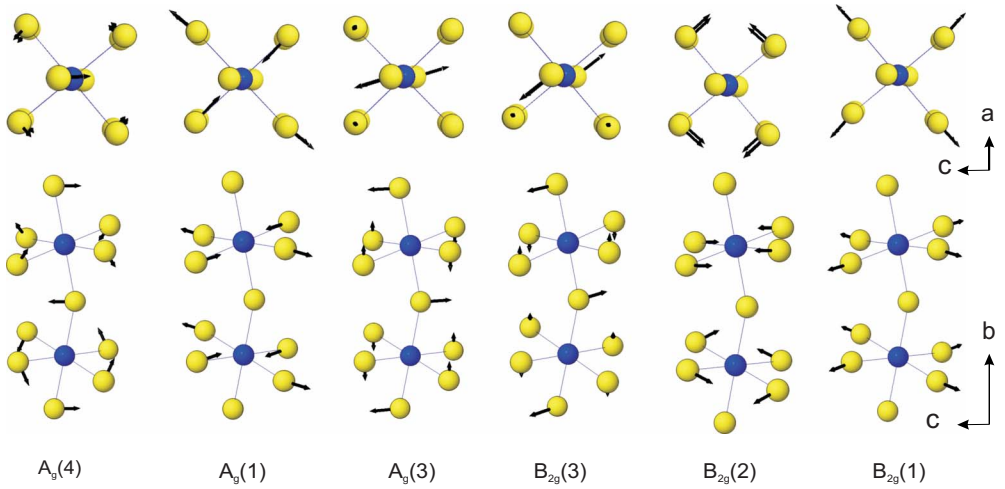

FIG. 2. (Color online) Main atomic-displacement patterns of the MnO_6 octahedra in the Raman active eigenmodes experimentally observed in Fig. 1. The mode patterns are adapted from Refs. 5 and 20. These were obtained from dynamical lattice calculations for $LaMnO_3$.

average ionic radius upon Y incorporation in $EuMnO_3$. Thus the same effects that are obtained for a decrease in rare-earth radius in stoichiometric $RMnO_3$ systems should be observable: a shift of most Raman active phonons to higher frequencies and mode mixing for $A_g(1)$ and $A_g(3)$ modes.[6] Both can be clearly seen for the results at $T=10$ K in Fig. 1 and are also present at room temperature. The shift of phonon frequencies depending on the Y content is depicted in Fig. 4, clearly showing a one-mode behavior for the Raman active phonon modes which consist almost exclusively of oxygen motions (see also Fig. 2). It can also be seen by comparison with data for pure $RMnO_3$ that $Eu_{1-x}Y_xMnO_3$ $(0 \leq x \leq 0.5)$ covers the range of $RMnO_3$ between $EuMnO_3$ and $TbMnO_3$.[6,8]

Spin-phonon coupling, which is the main objective of this study, is expected to manifest itself through an anomalous temperature dependence of the phonon frequencies in the temperature range of the magnetic ordered phases.[12–14] The T dependence of the $A_g(4)$, $A_g(1/3)$, $A_g(3/1)$, and $B_{2g}(1)$ phonon frequencies is shown in Fig. 5. The (red) solid lines correspond to the modeling function

$$\omega(T) = \omega_0 - C\left(1 + \frac{2}{\exp^{\hbar\omega_0/kT} - 1}\right), \qquad (1)$$

which describes the expected temperature dependence of the phonon frequency solely based on phonon-phonon decay.[22]

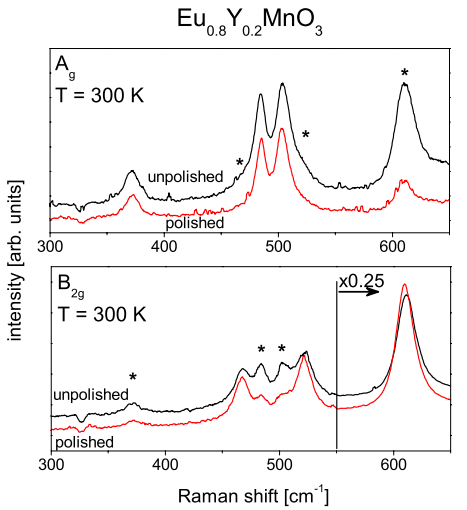

FIG. 3. (Color online) Polarized Raman spectra of a polished and an unpolished part of $Eu_{0.8}Y_{0.2}MnO_3$ obtained at $T=300$ K. The spectra were obtained under the same scattering configurations as in Fig. 1.

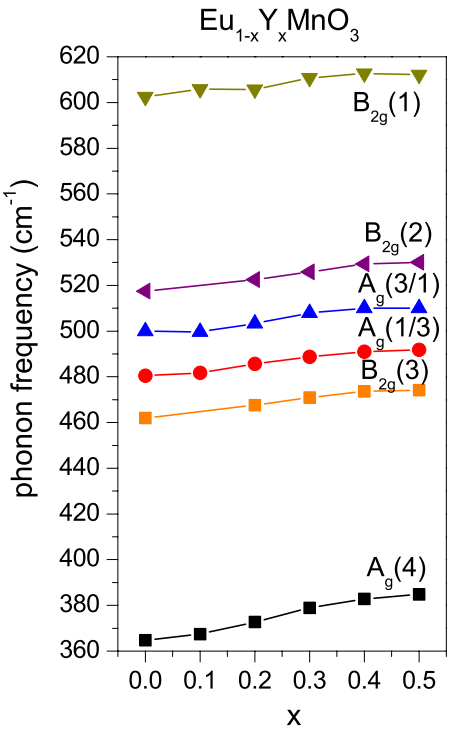

FIG. 4. (Color online) Shift of the phonon frequencies of $Eu_{1-x}Y_xMnO_3$ obtained at $T=10$ K with respect to the Y content x. Due to the very weak signal the $B_{2g}(2)$ and $B_{2g}(3)$ phonons could not be fitted in $Eu_{0.9}Y_{0.1}MnO_3$ (see text for further explanations).

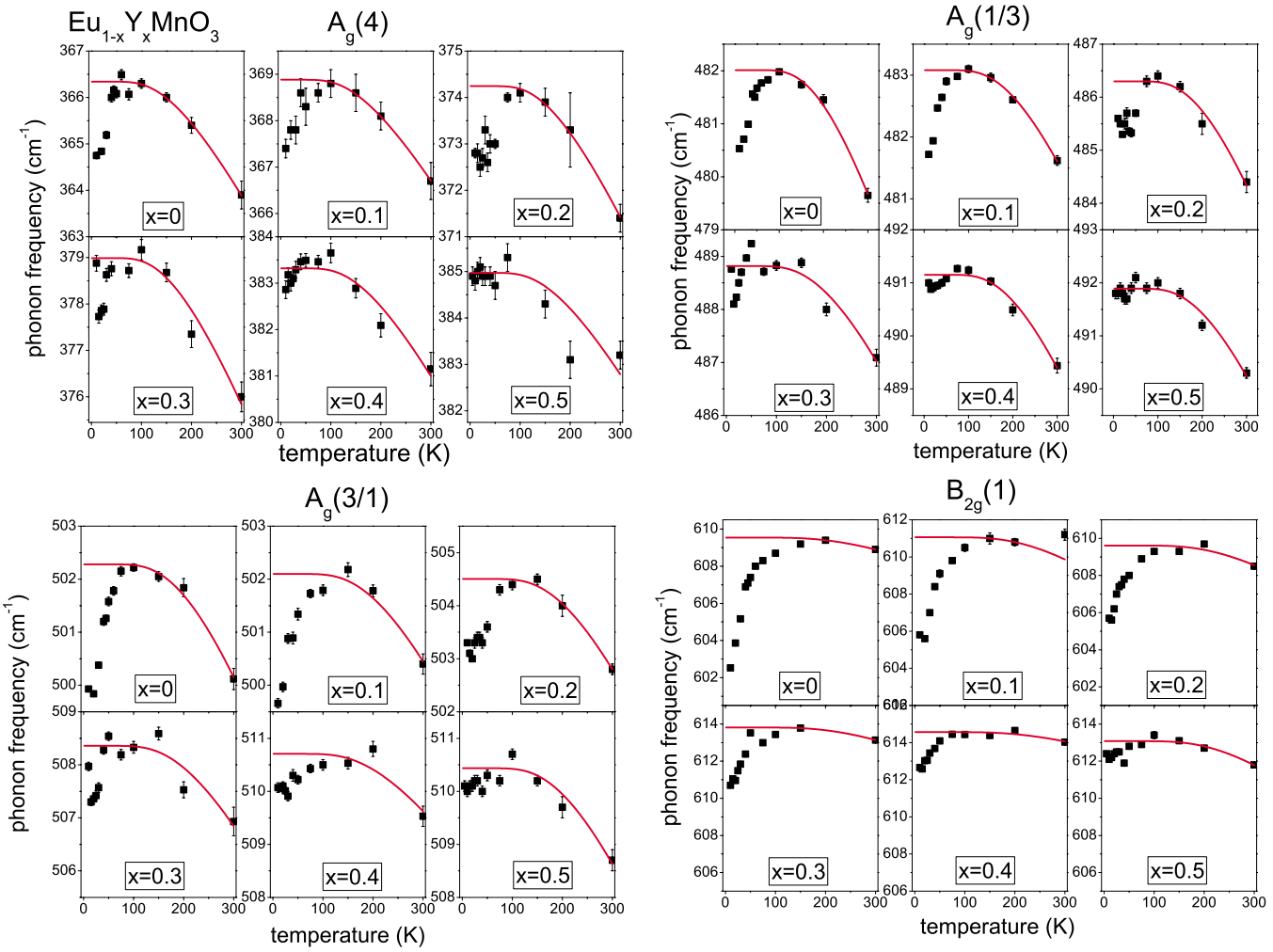

FIG. 5. (Color online) Temperature dependence of the $A_g(4)$, $A_g(1/3)$, $A_g(3/1)$, and $B_{2g}(1)$ phonon frequencies of $Eu_{1-x}Y_xMnO_3$ from $x=0$ to $x=0.5$, respectively. Solid (red) lines correspond to Eq. (1).

The parameters ω_0 and C were optimized for fitting the experimental data for $T>T_N$. Excellent agreement is obtained in the temperature range above $T\approx 100$ K.

Obviously in the temperature range below $T\approx 100$ K, a significant deviation from the behavior predicted by Eq. (1) occurs. A softening of the phonon frequencies is clearly visible, whose value depends on the sample composition as well as on the individual phonon mode. Considering the compositional dependence, the most pronounced softening occurs for pure $EuMnO_3$. Increasing Y content induces a monotonous decrease in the softening. Among the different phonon modes, the in-plane symmetric stretching mode $B_{2g}(1)$ is most strongly affected ($\Delta\omega/\omega\approx -1.1\%$). The $A_g(4)$, $A_g(1/3)$, and $A_g(3/1)$ phonons soften about a factor 2–3 weaker.

Similar softening was reported for several other $RMnO_3$ compounds, such as $LaMnO_3$,[23] $PrMnO_3$, $NdMnO_3$, and $SmMnO_3$ (Ref. 12) but not for $EuMnO_3$. Interestingly, previous investigations on the latter have shown a behavior according to Eq. (1).[12] This seemingly contradicting observation might be due to the fact that our phonon investigations are on nonpolycrystalline mixed crystals of $Eu_{1-x}Y_xMnO_3$ while the previous experiments were done on polycrystalline samples[12] and ceramics.[15]

The observed phonon softening for stoichiometric $RMnO_3$ systems is connected with the onset of an *A*-type AFM magnetic phase.[12,23] As mentioned earlier the magnetic phases depend on the rare-earth element. Orthorhombic $RMnO_3$ compounds with relative large rare-earth ion radius (La^{3+}, Pr^{3+}, Nd^{3+}, Sm^{3+}) possess an *A*-type AFM order where ferromagnetic layers of Mn^{3+} ions in the *ac* plane (MnO_2 plane) are coupled antiferromagnetically along the *b* axis (in *Pnma* notation).[9] With decreasing rare-earth ion radius the orthorhombic distortion (tilting and buckling of the MnO_6 octahedra) increases, leading to shortened nearest-neighbor (NN) and next-nearest-neighbor (NNN) distances between Mn^{3+} ions. This causes an increasing importance of magnetic exchange between NNN Mn^{3+}. The exchange path for NNN along the *a* axis is Mn-O-O-Mn and is antiferromagnetic. Therefore the ferromagnetic interaction in the *ac* layers is weakened, which clearly correlates with the decrease in the Néel temperature from $T_N=145$ K for $LaMnO_3$ to $T_N=60$ K for $SmMnO_3$, whose R^{3+} radius is smaller by $\approx 7\%$. Further reduction in the rare-earth ion radii by employing Eu^{3+}, Gd^{3+}, and Tb^{3+}, whose radii correspond to our sample series, leads to the appearance of an incommensurate sinusoidal spin structure at intermediate temperatures.[9] This spin

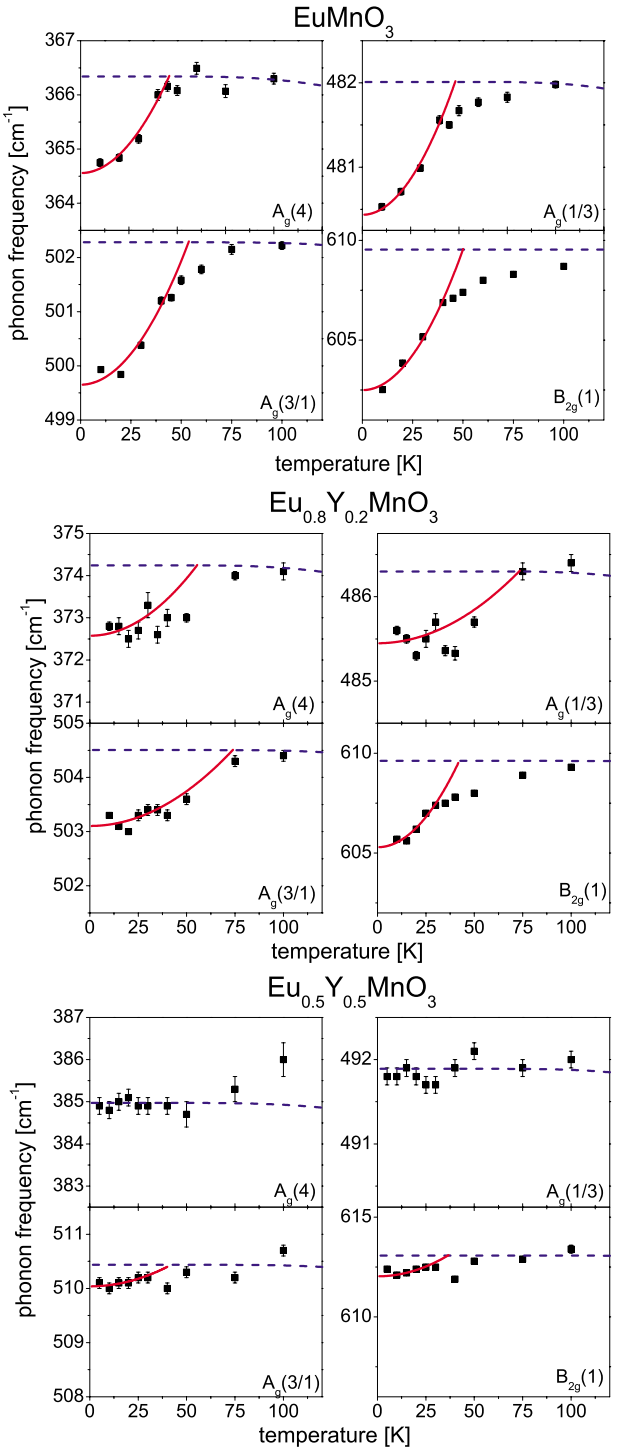

FIG. 6. (Color online) Phonon softening of all analyzed phonon modes of $EuMnO_3$, $Eu_{0.8}Y_{0.2}MnO_3$, and $Eu_{0.5}Y_{0.5}MnO_3$. The dashed (blue) lines correspond to a fit using Eq. (1) and the solid (red) line corresponds to a parabola fit for $T \leq T_N$. For $Eu_{0.5}Y_{0.5}MnO_3$ only the $A_g(3/1)$ and the $B_{2g}(1)$ phonon modes were fitted due to the small phonon shifts.

structure is characterized by a propagation vector $\mathbf{k}=(k_x,0,0)$ which is temperature dependent. For $EuMnO_3$ and $GdMnO_3$ yet a canted A-type AFM order develops below $T_N=46$ K and $T_N=26$ K, respectively. In $TbMnO_3$ no A-type AFM order is observed in zero external magnetic fields. Instead a spiral magnetic structure with a temperature-independent $\mathbf{k}$ develops.

The magnetic and dielectric phases of the nonstoichiometric $Eu_{1-x}Y_xMnO_3$ system ($0 \leq x \leq 0.5$) were systematically studied in literature.[7,8] It was shown that the behavior is very similar to that of the stoichiometric nondoped $RMnO_3$ compounds, apart from the very low-temperature region ($T < 10$ K) where the ordering of the magnetic moments of the rare-earth ions occurs. The paramagnetic regime above $T_N \approx 45-50$ K is followed upon cooling by a sinusoidal collinear magnetic structure of the manganese spins. For small Y concentrations ($x=0$ and $x=0.1$) at $T \leq 45$ and 35 K, respectively, a small ferromagnetic moment along the b axis was detected and thus the existence of a canted A-type AFM phase was concluded. For $Eu_{0.8}Y_{0.2}MnO_3$ also a small ferromagnetic moment along the b axis occurs, which points to the existence of an A-type AFM. However in this sample multiferroicity exists and due to theoretical arguments a collinear magnetic structure cannot occur. Therefore Hemberger *et al.*[8] proposed a conelike structure, which breaks inversion symmetry and carries a weak ferromagnetic moment along the b axis. For higher Y concentrations ($x \geq 0.3$) the weak ferromagnetic moment along the b axis vanishes and a noncollinear spiral magnetic phase occurs. It is not clear if this magnetic ground state is truly incommensurate or commensurate with a long-range magnetic wavelength.

From literature[12] and our results it is clear, that in $RMnO_3$ crystals with A-type AFM ordering spin-phonon coupling is particularly strong. Granado *et al.*[23] proposed a mechanism of phonon renormalization which is proportional to the spin-spin correlation function $\langle \mathbf{S_i} \cdot \mathbf{S_j} \rangle$ for the NN spins localized at the Mn^{3+} ions. The following expression for phonon renormalization was obtained:

$$\Delta\omega = -\frac{1}{2\mu_\alpha \omega_\alpha} \sum_{i,j>i} \frac{\partial^2 J_{ij}}{\partial u_\alpha^2} \langle \mathbf{S_i} \cdot \mathbf{S_j} \rangle, \tag{2}$$

where J_{ij} is the magnetic exchange energy between the ith and the jth Mn^{3+} spins, ω_α the mode frequency of phonon α, μ_α the reduced mass for the corresponding phonon, and u_α the oxygen displacement. The sum runs over all next-nearest neighbors j of the ith Mn^{3+} avoiding double counting. In a simplified picture the spin-phonon coupling can be considered as a dynamic modulation of the magnetic exchange constant J_{ij} due to the Raman active phonon mode α which is obtained by a second-order Taylor expansion of the displacement of the O^{2-}. The spin-spin correlation function $\langle \mathbf{S_i} \cdot \mathbf{S_j} \rangle$ is expressed within the molecular field approximation yielding $\langle \mathbf{S_i} \cdot \mathbf{S_j} \rangle \approx 4[M_{sublatt}(T)/4\mu_B]^2$ where $M_{sublatt}(T)$ is the sublattice magnetization within the MnO_2 plane per Mn^{3+} ion. Considering the in-plane symmetric stretching mode $B_{2g}(1)$ phonon, the reduced mass can be replaced by the oxygen mass m and the following expression is obtained:[23]

$$\Delta\omega = -\frac{2}{m\omega} \frac{\partial^2 J_{\mathrm{NN}}}{\partial u_{xz}^2} \left[\frac{M_{sublatt}(T)}{4\mu_B} \right]^2. \tag{3}$$

The phonon renormalization scaling $\propto M^2$ was shown to be a good approximation for *A*-type AFM materials (R=La, Pr, Nd, and Sm). With Eq. (3) the temperature behavior of the phonon modes below T_N could be nicely fitted in the literature[12,23] and, as will be seen in the following, also our experimental data (see Fig. 6).

As it is also argued by Laverdière *et al.*,[12] the *i*th spin can be represented as

$$\mathbf{S}_i = \frac{\mathbf{M}}{4\mu_B} + \Delta\mathbf{S_i}, \tag{4}$$

where $\mathbf{M}$ is the average sublattice magnetization per Mn^{3+} and $\Delta\mathbf{S_i}$ is the spin fluctuation due to quantum and thermal effects.

As is evident from the existing data the strength of the renormalization is mode dependent. Additionally, the onset of the renormalization occurs already above T_N and is also mode sensitive. For $B_{2g}(1)$ in $EuMnO_3$ as the most pronounced example the frequency softening is the strongest ($\Delta\omega/\omega \approx -1.1\%$). The softening starts at $T \approx 150$ K and has an inclination point at T_N=45 K. For the other phonon modes the softening is less pronounced and starts at lower temperatures. This fact can be explained by locally correlated spin fluctuations $\Delta\mathbf{S}_i$ in the ferromagnetically ordered MnO_2 plane which do occur even in the paramagnetic region. Therefore, phonon modes with in-plane oxygen displacement in the MnO_2-plane shift their frequency by a larger amount and are more sensitive to these fluctuations than modes with out-of-plane and (apical) oxygen movement in the Eu(Y)O plane. This is clearly reflected in the temperature behavior of the phonon modes depicted in Fig. 6. Comparison of the mode patterns shown in Fig. 2 leads to the expectance that the $B_{2g}(1)$ and $A_g(1)$ phonon modes should have the most pronounced frequency shift and should be very sensitive to spin fluctuations in the MnO_2 plane. For $B_{2g}(1)$ this is nicely verified while $A_g(1)$ shows a behavior similar to the $A_g(3)$ mode which only weakly modulates the in-plane Mn-O-bonds. This can be understood by the mode-mixing effect between $A_g(1)$ and $A_g(3)$ for $RMnO_3$ systems with (average) rare-earth radii in the region of Eu^{3+}, Gd^{3+}, and Tb^{3+}.[6] Thus less pronounced frequency shifts and sensitivity to spin fluctuations within the MnO_2 plane are obtained for these two modes. Finally $A_g(4)$, which has mainly components perpendicular to the MnO_2 plane, has a small frequency shift and almost no fluctuation-induced renormalization effects above T_N.

As is evident from Figs. 5 and 6, the phonon softening also occurs, although with reduced amplitude, for the non *A*-type AFM samples with x=0.3, 0.4, and 0.5. The data shown in Fig. 6 can be fitted according to the same procedure as for stoichiometric $EuMnO_3$. For example, for $B_{2g}(1)$ the phonon softening is reduced from $\Delta\omega/\omega \approx -1.1\%$ in $EuMnO_3$ to $\Delta\omega/\omega \approx -0.2\%$ in $Eu_{0.5}Y_{0.5}MnO_3$. For an explanation of this behavior an extended model of spin-phonon coupling is needed. This was developed by Laverdière *et al.*[12] to include the cases of incommensurate and *E*-type AFM ordering. For an incommensurate magnetic phase with wave vector $\mathbf{k}=(k_x,0,0)$ ($x=a$ axis) they write the spin-spin correlation as

$$\langle \mathbf{S_i} \cdot \mathbf{S_j} \rangle = K(T)\cos(2\pi\mathbf{k}\cdot\mathbf{r}), \tag{5}$$

where $K(T)$ is a temperature-dependent prefactor, which gives the degree of magnetic ordering against thermal disorder. Its maximum value is located at T=0 K and it is decreasing with increasing temperature. For $T > T_N$ it approaches zero, expressing the vanishing of the long-range magnetic ordering. $\mathbf{r}$ is the distance between adjacent Mn^{3+} ions. For NN spins ($\mathbf{r} = \pm\mathbf{a}/2 \pm \mathbf{c}/2$) a ferromagnetic coupling $J=J_1<0$ occurs, while the coupling for NNN ($\mathbf{r} = \pm\mathbf{a}$) is antiferromagnetic, $J=J_2>0$, and for NNN ($\mathbf{r} = \pm\mathbf{c}$) an additional very weak ferromagnetic coupling, $J=J_3<0$, exists. Thus summing up to NNN Mn^{3+} the phonon renormalization can be expressed as

$$\Delta\omega = -\frac{1}{2\mu_\alpha\omega_\alpha}\sum_{i,j>i}\frac{\partial^2 J_{ij}}{\partial u_\alpha^2}\langle \mathbf{S_i}\cdot\mathbf{S_j}\rangle$$

$$= \frac{K(T)}{m\omega}[2D_1\cos(\pi k_x) + D_2\cos(2\pi k_x) + D_3], \tag{6}$$

where D_k (k=1,2,3) describes the second derivative of the magnetic exchange constant J_{ij} of NN (J_1), NNN (J_2), and NNN (J_3) Mn^{3+} spins with respect to the oxygen displacement. The temperature dependence is expressed through the temperature-dependent prefactor $K(T)$ of the spin-spin correlation, thus D_k is considered as temperature independent. The *A*-type AFM ordering is obtained for $\mathbf{k}=0$, $K(T) \propto M^2_{sublatt}$ leading to Eq. (3).

The dependence of the J_{ij} on the Mn-O-Mn tilting angle is elucidated by mean-field calculations on a two-dimensional square lattice in Ref. 9. These calculations show that for a decreasing tilting angle (i.e., deviation of the Mn-O-Mn angle from 180°) a drastic increase of NNN J_2 (from weak FM to strong AFM) is induced resulting in a change in the macroscopic magnetic structure from *A*-type AFM via incommensurate magnetic ordering toward *E*-type AFM. This compensation of the FM interaction in the MnO_2 layers can be detected by a decrease in phonon softening in Raman measurements. Additionally in the mixed crystals $Eu_{1-x}Y_xMnO_3$ investigated here the randomness of the incorporated Y ions has to be considered leading to a distribution of the lattice distortion which causes the magnetic frustration and thus the incommensurate magnetic structure at higher Y contents. This will be discussed later. An effective spin-phonon coupling constant D_{eff} is therefore introduced summing up contributions from all D_k and we get for the phonon renormalization

$$\Delta\omega = \frac{K(T)}{m\omega}D_{eff} \tag{7}$$

with $D_{eff}=2D_1\cos(\pi k_x)+D_2\cos(2\pi k_x)+D_3$. In the following the symmetric stretching mode $B_{2g}(1)$ will be considered. In literature the temperature-dependent prefactor for canted *A*-type AFM phases was obtained by the sublattice magnetization values obtained from neutron diffraction.[12] For obtaining $K(T)$ for canted *A*-type AFM $Eu_{1-x}Y_xMnO_3$ (Y content $x \leq 0.2$) one can utilize the results of magnetization measurements along the *b* axis of Hemberger *et al.*[8] to calculate the in-plane sublattice magnetization. However for in-

TABLE I. Quantitative phonon softening $\Delta\omega$ extrapolated to $T=0$ K from the fits shown exemplary in Fig. 6 as well as the numerical results for D_{eff} obtained from Eq. (7). Both are compared with literature. As for Y doping $x>0.2$ no data of sublattice magnetization could be obtained, only $\Delta\omega$ is shown.

Sample	$\Delta\omega$ (cm^{-1})	$\mu_{unit\ cell}$ (μ_B)	D_{eff} (mRy/Å^2)
$LaMnO_3$	8.0[e]	3.65[a]	16[e]
$PrMnO_3$	6.5[b]	3.5[b]	15.5[b]
$NdMnO_3$	6.0[b]	3.22[c]	13.5[b]
$SmMnO_3$	5.5[b]	3.5[d]	12.9[b]
$EuMnO_3$	6.5	4[f]	13.4
$Eu_{0.9}Y_{0.1}MnO_3$	5.6	4[f]	11.6
$Eu_{0.8}Y_{0.2}MnO_3$	4.2	4[f]	8.6
$Eu_{0.7}Y_{0.3}MnO_3$	3.2		
$Eu_{0.6}Y_{0.4}MnO_3$	2.0		
$Eu_{0.5}Y_{0.5}MnO_3$	1.2		

[a]Values taken from Ref. 24.
[b]Reference 12.
[c]Reference 25.
[d]Reference 26.
[e]Reference 23.
[f]Reference 8.

commensurate magnetic phases ($x>0.2$) we have no macroscopic magnetization caused by a slightly canted AFM ordering of the Mn^{3+} spins. Thus in Table I we compare the phonon softening of the stochiometric $RMnO_3$ compounds from Refs. 12 and 23 with the phonon softening of our whole $Eu_{1-x}Y_xMnO_3$ sample series. As was done in these papers, Eq. (7) can be used to obtain numerical values for the D_{eff}. Our numerical values of D_{eff} for $x\leq 0.2$ (where sublattice magnetization data could be obtained) as well as the maximum strength of the frequency shift $\Delta\omega$ are listed in Table I and compared to literature.

The trend of a very moderate weakening of the spin-phonon coupling constant D_{eff} with decreasing rare-earth ionic radii, which is reported for stoichiometric A-type AFM $RMnO_3$,[12] is confirmed in the $Eu_{1-x}Y_xMnO_3$ system.

In principle, two scenarios might be responsible for this behavior. In the first scenario phase separation is assumed and thus local canted A-type antiferromagnetic domains could be still possible though a macroscopic magnetic moment would be not detectable due to the random distribution of the domains. We rule out this scenario for two reasons: (i) as shown in Ref. 8 the magnetization measurements should show a weak ferromagnetic moment along the b axis. In case of domains, these should have been aligned in the B field, resulting in a finite value for the macroscopic magnetization. (ii) Additionally a phase separation should lead to clustering of the incorporated Y ions thus causing $YMnO_3$-like domains in $EuMnO_3$. The Raman active phonons which are sensitive to a change in the Mn-O-Mn bending angle [the MnO_6 bending and tilting modes, e.g., $A_g(4)$, $A_g(1/3)$, or $B_{2g}(3)$] should show a two-mode behavior, or at least an inhomogeneous broadening in this scenario. This is not observed (see Figs. 1 and 4) for the Raman active phonons. However we would like to stress here the main difference between the stoichiometric compounds studied in literature and our mixed crystals. Due to Y doping a random distribution of Y ions is incorporated in $EuMnO_3$ leading to an inherent distribution of the lattice distortion of the MnO_6 octahedra, e.g., the Mn-O-Mn tilting angle. Though in our measurements we did not detect effects on the Raman active phonons (such as inhomogeneous broadening) one has to consider that for explaining the phonon softening a model is employed which sums up not only NN Mn^{3+} spins but also NNN. This leads to a correlation length of the spin-phonon coupling which is clearly larger than one unit cell. Thus, phonons are a local probe for the spin-phonon coupling but on a correlation length scale larger than a single unit cell. This allows us to adopt an "effective-medium approximation" on the scale of a few unit cells without having to average over the whole crystal.

The second scenario is the base of our numerical calculations: even in an incommensurate magnetic phase there still is a significant spin-phonon coupling because the spin-phonon coupling is an effect caused by locally correlated spins, which is persistent in the incommensurate magnetic phase although the macroscopic magnetic moment connected with the canted A-type AFM phase vanishes. Therefore we conclude that even in the case of a long-range modulated spin structure the model of Laverdière *et al.*[12] is still applicable. The reduction in the spin-phonon coupling constant D_{eff} is originating from the compensation of the ferromagnetic NN exchange (D_1) with the antiferromagnetic NNN exchange (D_2). The finite remaining value is therefore not connected to the existence of an A-type AFM but to a local correlation of the Mn^{3+} spins within the MnO_2 plane. An additional factor responsible for the weakening of the phonon softening is the tilting of the Mn^{3+} spins along the a axis associated with the wave vector of the spiral magnetic phase, which lifts the degeneracy of the four NN Mn^{3+} spins within the MnO_2 plane thus reducing the net magnetic moment of the Mn^{3+} spins within the unit cell.

IV. CONCLUSION

In summary, we have investigated the temperature-dependent polarized Raman spectra of single crystalline orthorhombic $Eu_{1-x}Y_xMnO_3$ ($0\leq x\leq 0.5$). Our results show that for pure $EuMnO_3$ a strong spin-phonon coupling within the MnO_2 plane exists, manifesting itself by a softening of the phonon modes, whose eigendisplacements have components, that modulate bonds within this plane. It is most pronounced for the $B_{2g}(1)$ symmetric in-plane stretching mode. The coupling is reduced by the increasing incorporation of Y. One can describe this behavior by local spin-spin correlation leading to the microscopic origin of the phonon renormalization —the modulation of magnetic exchange by a phonon mode. The spin-phonon coupling is detectable even in an incommensurate spiral magnetic phase. For known sublattice magnetization within the MnO_2 plane the estimation

of the corresponding effective spin-phonon coupling constant $\partial^2 J_{eff}/\partial u^2$ of the $B_{2g}(1)$ mode was carried out. These quantitative results show the importance of phonons as a probe for spin-spin correlations within this material class.

ACKNOWLEDGMENT

One of the authors (S.I.) would like to acknowledge financial support of the Studienstiftung des deutschen Volkes e.V.

*sven.issing@physik.uni-wuerzburg.de

[1] M. Fiebig, J. Phys. D **38**, R123 (2005).
[2] S. W. Cheong and M. Mostovoy, Nature Mater. **6**, 13 (2007).
[3] T. Kimura, T. Goto, H. Shintani, K. Ishizaka, T. Arima, and Y. Tokura, Nature (London) **426**, 55 (2003).
[4] T. Goto, T. Kimura, G. Lawes, A. P. Ramirez, and Y. Tokura, Phys. Rev. Lett. **92**, 257201 (2004).
[5] M. N. Iliev, M. V. Abrashev, H.-G. Lee, V. N. Popov, Y. Y. Sun, C. Thomsen, R. L. Meng, and C. W. Chu, Phys. Rev. B **57**, 2872 (1998).
[6] M. N. Iliev, M. V. Abrashev, J. Laverdiere, S. Jandl, M. M. Gospodinov, Y.-Q. Wang, and Y.-Y. Sun, Phys. Rev. B **73**, 064302 (2006).
[7] V. Yu. Ivanov, A. A. Mukhin, V. D. Travkin, A. S. Prokhorov, Yu. F. Popov, A. M. Kadomtseva, G. P. Vorob'ev, K. I. Kamilov, and A. M. Balbashov, Phys. Status Solidi B **243**, 107 (2006).
[8] J. Hemberger, F. Schrettle, A. Pimenov, P. Lunkenheimer, V. Y. Ivanov, A. A. Mukhin, A. M. Balbashov, and A. Loidl, Phys. Rev. B **75**, 035118 (2007).
[9] T. Kimura, S. Ishihara, H. Shintani, T. Arima, K. T. Takahashi, K. Ishizaka, and Y. Tokura, Phys. Rev. B **68**, 060403(R) (2003).
[10] A. Pimenov, A. Mukhin, V. Y. Ivanov, V. D. Travkin, A. M. Balbashov, and A. Loidl, Nat. Phys. **2**, 97 (2006).
[11] A. Pimenov, T. Rudolf, F. Mayr, A. Loidl, A. A. Mukhin, and A. M. Balbashov, Phys. Rev. B **74**, 100403(R) (2006).
[12] J. Laverdiere, S. Jandl, A. A. Mukhin, V. Y. Ivanov, V. G. Ivanov, and M. N. Iliev, Phys. Rev. B **73**, 214301 (2006).
[13] A. F. Garcia-Flores, E. Granado, H. Martinho, R. R. Urbano, C. Rettori, E. I. Golovenchits, V. A. Sanina, S. B. Oseroff, S. Park, and S.-W. Cheong, Phys. Rev. B **73**, 104411 (2006).
[14] A. F. Garcia-Flores, E. Granado, H. Martinho, C. Rettori, E. I. Golovenchits, V. A. Sanina, S. B. Oseroff, S. Park, and S.-W. Cheong, J. Appl. Phys. **101**, 09M106 (2007).
[15] W. S. Ferreira, J. A. Moreira, A. Almeida, M. R. Chaves, J. P. Araújo, J. B. Oliveira, J. M. Machado Da Silva, M. A. Sá, T. M. Mendonça, P. S. Carvalho, J. Kreisel, J. L. Ribeiro, L. G. Vieira, P. B. Tavares, and S. Mendonça, Phys. Rev. B **79**, 054303 (2009).
[16] A. M. Balbashov, S. G. Karabashev, Y. M. Mukovskiy, and S. A. Zverkov, J. Cryst. Growth **167**, 365 (1996).
[17] A. Pimenov, A. Loidl, A. A. Mukhin, V. D. Travkin, V. Y. Ivanov, and A. M. Balbashov, Phys. Rev. B **77**, 014438 (2008).
[18] A. Pimenov, A. M. Shuvaev, A. A. Mukhin, and A. Loidl, J. Phys.: Condens. Matter **20**, 434209 (2008).
[19] P. Yu and M. Cardona, *Fundamentals of Semiconductors*, 3rd ed. (Springer, New York, 2001).
[20] I. S. Smirnova, Physica B **262**, 247 (1999).
[21] S. Koritnig, *Landolt-Börnstein: Numerical Data and Functional Relationships in Science and Technology*, 6th ed. (Springer, Berlin, 1955), Vol. I.
[22] M. Balkanski, R. F. Wallis, and E. Haro, Phys. Rev. B **28**, 1928 (1983).
[23] E. Granado, A. García, J. A. Sanjurjo, C. Rettori, I. Torriani, F. Prado, R. D. Sánchez, A. Caneiro, and S. B. Oseroff, Phys. Rev. B **60**, 11879 (1999).
[24] Q. Huang, A. Santoro, J. W. Lynn, R. W. Erwin, J. A. Borchers, J. L. Peng, and R. L. Greene, Phys. Rev. B **55**, 14987 (1997).
[25] A. Muñoz, J. A. Alonso, M. J. Martínez-Lope, J. L. García-Muñoz, and M. T. Fernández-Díaz, J. Phys.: Condens. Matter **12**, 1361 (2000).
[26] V. Yu. Ivanov, A. A. Mukhin, A. S. Prokhorov, and A. M. Balbashov, Phys. Status Solidi B **236**, 445 (2003).